TISSUE ENGINEERING: Part A
Volume 21, Numbers 5 and 6, 2015

DOI: 10.1089/ten.tea.2014.0163

Biocompatibility of Tungsten Disulfide Inorganic Nanotubes and Fullerene-Like Nanoparticles with Salivary Gland Cells

Elisheva B. Goldman, MSc,[1,2] Alla Zak, PhD,[3] Reshef Tenne, PhD,[2] Elena Kartvelishvily, PhD,[4] Smadar Levin-Zaidman, PhD,[4] Yoav Neumann, PhD (Cand),[1] Raluca Stiubea-Cohen, PhD (Cand),[1] Aaron Palmon, DMD, PhD,[1] Avi-Hai Hovav, PhD,[1] and Doron J. Aframian, DMD, PhD[1]

Impaired salivary gland (SG) function leading to oral diseases is relatively common with no adequate solution. Previously, tissue engineering of SG had been proposed to overcome this morbidity, however, not yet clinically available. Multiwall inorganic (tungsten disulfide [WS_2]) nanotubes (INT-WS_2) and fullerene-like nanoparticles (IF-WS_2) have many potential medical applications. A yet unexplored venue application is their interaction with SG, and therefore, our aim was to test the biocompatibility of INT/IF-WS_2 with the A5 and rat submandibular cells (RSC) SG cells. The cells were cultured and subjected after 1 day to different concentrations of INT-WS_2 and were compared to control groups. Growth curves, trypan blue viability test, and carboxyfluorescein succinimidyl ester (CFSE) proliferation assay were obtained. Furthermore, cells morphology and interaction with the nanoparticles were observed by light microscopy, scanning electron microscopy and transmission electron microscopy (TEM), and energy dispersive X-ray spectroscopy. The results showed no significant differences in growth curves, proliferation kinetics, and viability between the groups compared. Moreover, no alterations were observed in the cell morphology. Interestingly, TEM images indicated that the nanoparticles are uptaken by the cells and accumulate in cytoplasmic vesicles. These results suggest promising future medical applications for these nanoparticles.

Introduction

Various nanoparticle types are gaining importance for their clinical applications, such as disease diagnosis, fluorescent biological labels, antibody and DNA probes, detection of pathogens, protein chips, drug delivery agents, cardiac therapy, as well as dental care.[1] Inorganic nanotubes (INT) and fullerene-like (IF) nanoparticles are hollow polyhedral structures first observed two decades ago.[2,3] They could be synthesized from a number of inorganic layered van der Waals materials, such as molybdenum disulfide (MoS_2) or tungsten disulfide (WS_2). This discovery opened a new field of inorganic solid-state chemistry, which subsequently developed in many directions.

The structure of the IF and INT is analogous to that of multiwall carbon fullerenes and nanotubes. In their original morphology, layered materials consist of two-dimensional molecular sheets stacked and held together by van der Waals forces. Due to the abundant dangling bonds of the rim atoms, they are not stable as two-dimensional nanoplatelets. By folding along one direction, multiwall nanotubes are generated, while folding along two axes leads to hollow quasispherical nanostructures termed fullerene-like.[4] The diameter of the WS_2 fullerene-like nanoparticles (IF-WS_2) is between 120 and 150 nm. The dimensions of the WS_2 nanotubes (INT-WS_2) are 40–150 nm in diameter, with an average of $\sim$75 nm, and 1–10 μm in length, although they can break while handling them, leading to a shorter diameter.

These nanomaterials have been shown to exhibit superior mechanical and tribological properties,[5–7] and their possible applications include solid-state lubrication in automotive and aerospace industries, reinforcing polymers by preparation of nanocomposites, high-energy density batteries, sensors, photoconversion of solar energy, and nanoelectronics.[4] Indeed, a significant amount of products based on this nanotechnology were recently commercialized. In the biomedical field, INT and IF are studied for various applications; IF and INT of different compounds can be functionalized with proteins and other biomolecules, making them potential candidates as targeted drug delivery carriers or for bioimaging.[8–10] For example, the

[1]Faculty of Dental Medicine, The Hebrew University of Jerusalem, Jerusalem, Israel.
[2]Department of Materials and Interfaces, Weizmann Institute of Science, Rehovot, Israel.
[3]Faculty of Science, Holon Institute of Technology, Holon, Israel.
[4]Electron Microscopy Unit, Weizmann Institute of Science, Rehovot, Israel.

surface of fullerene-like rhenium disulfide nanoparticles (IF-ReS_2) was immobilized with porphyrin molecules, which can be excited by near UV-visible light and fluoresce. This is the basis for a proposed photodynamic therapeutic treatment for several kinds of cancer.[10,11] Titanium oxide (TiO_2) nanotubes were found to be effective for photodynamic therapeutic cancer treatment, as well.[12] The mechanical properties of the INT-WS_2 have led to research in the direction of reinforcing scaffolds for tissue engineering.[13] TiO_2 nanotubes, due to their ability to enhance positive cellular response, were studies for implantation purposes.[14] In addition, the unique tribological properties of IF-WS_2 have led to research in the direction of gels[15] or coatings for medical devices, such as orthodontic wires, endodontic files, catheters, stents,[11] as well as artificial joints,[16] for the purpose of friction reduction. Moreover, Re:IF-MoS_2 (rhenium-doped fullerene-like MoS_2) reduced the attachment of encrustation stones on ureteral stents and catheters.[17] In another study, $(BiO)_2CO_3$ nanotubes were shown to exhibit a very strong antibacterial reactivity toward *Helicobacter pylori*.[18] A recent novel study suggested that due to their piezoelectric properties, boron nitride nanotubes (BNNT) can serve as carriers for targeted electrical stimuli to neuronal cells.[19]

However, the first step to applying any new nanomaterial in the medical field requires biocompatibility testing. The biocompatibility research of IF and INT nanoparticles is in a preliminary stage, and so far, the results differ depending on the nanoparticle type.

TiO_2 nanotubes and BNNT biocompatibility was tested in several studies *in vitro* and *in vivo,*[14,20] and the results indicated generally a positive biocompatible effect depending on the type of nanoparticle. The biocompatibility of IF-MoS_2 and IF-WS_2 were tested *in vitro* and the results were encouraging, indicating that IF-MoS_2 are biocompatible.[21–23] IF-WS_2 were tested on rats through inhalation, digestion, and dermal application, showing no sign of toxicity.[11] Moreover, a recent study tested the cytotoxicity of INT-WS_2 and IF-MoS_2 on bronchial, hepatic, and macrophage cells, and found them nontoxic.[24] An important issue in the assessment of biocompatibility is whether the nanoparticles induce an immune response. It was suggested in a recent article that the lower toxicity of INT-WS_2 and IF-WS_2 compared with other nanoparticles results from decreased proinflammatory activation on the one hand, and a comparable significant capacity to induce protective antioxidant/detoxification defense mechanisms on the other hand.[25]

Salivary gland (SG) secrete $\sim$500 mL of saliva daily, the *aqua vita* of the oral cavity. Saliva fulfills many functions to maintain the normal homeostasis of the oral cavity. There are several causes for SG impairment, including xerogenic drugs, autoimmune diseases, and radiation therapy. Impairment in salivary secretion leads to rampant dental caries, frequent mucosal infections, and difficulties in swallowing, chewing, and speech. Patients may also experience considerable pain and discomfort, all of which significantly decrease their quality of life.[26] Unfortunately, up to date, there is no satisfactory treatment for irreversible damage to the SG.[27] Novel but not yet clinically applicable strategies include adult SG stem cell autologous transplantation therapy leading to tissue regeneration[28,29] and utilizing an artificial SG device.[26–28,30–34]

As mentioned, due to these mechanical properties of nanoparticles, they may be potential candidates for reinforcement of scaffolds for artificial SG devices. In addition, other potential applications of IF/INT-WS_2 on SG-related disorders include the delivery of drugs and biomolecules specifically to the SG to decrease side effects or to deliver relevant growth factors specifically to certain stem cells, coating of devices introduced into the SG (as sialendoscopy) for friction reduction, cancer hypothermia treatment, and imaging contrast agents. The aim of the present study, therefore, was to test the biocompatibility of IF/INT-WS_2 with A5 rat submandibular ductal epithelial cell line[35] and rat submandibular cells (RSc) line expressing integrin $\alpha6\beta1$ (a progenitor cell marker),[29] as the first step toward future applications. We investigated their biocompatibility in three major aspects: their effect on cell proliferation, morphology, and their direct interaction with the cells.

Materials and Methods

INT-WS_2 and IF-WS_2 synthesis

For the large-scale IF/INT-WS_2 synthesis, a high temperature (800–900°C) process and fluidized bed reactor were used as previously described.[36,37] Briefly, tungsten oxide powder and H_2S gas served as the reaction precursors in a reducing atmosphere of hydrogen. Most remarkably, the synthesis of both IF and INT is done in the same reactor; however, each required its unique reaction conditions. The nanoparticles were provided by NanoMaterials, Ltd. Typical electron micrographs of these nanoparticles are shown in Figure 1.

Cell culture

A5 cells were provided by Prof. Bruce Baum (NICDR, NIH, Bethesda). The A5 cells were grown in Dulbecco's modified Eagle's medium (DMEM) supplemented with 10% fetal bovine serum, 1% L-glutamine, and 1% penicillin–streptomycin–amphotericin (PSA) solution, as previously described.[38] RSC cells were grown in a medium containing DMEM and F12 in a 1:1 ratio, supplemented with 10% fetal calf serum and 1% PSA, as previously described.[29] The cells were grown at 37°C in a humidified chamber containing 5% CO_2. The cells were detached using 0.25% trypsin EDTA (all products from Biological Industries).

Cell growth curves and trypan blue staining

A5 and RSC cells were seeded in 96-well tissue culture dishes at a density of 6.2×10^3 cells/cm^2. Twenty-four hours later, the medium of all wells was changed to fresh medium containing INT-WS_2 (for A5 cells) or IF-WS_2 (for RSC cells) in different concentrations (0.22, 3.52, and 35.2 μg/mL for the INT-WS_2; 35.2 and 100 μg/mL for the IF-WS_2). A control group containing no nanoparticle was seeded for each cell type as well.

The nanoparticles were disinfected by UV light overnight before they were added to the medium.

Twenty-four hours after the application of the nanoparticles, 4–12 wells from each group were dissociated daily until culture reached confluence and counted manually with a hemocytometer chamber. RSC cells were stained with trypan blue (BioWhittaker) in a 1:1 ratio before being counted. The growth curves plotted exclude the cells counted as ''dead.''

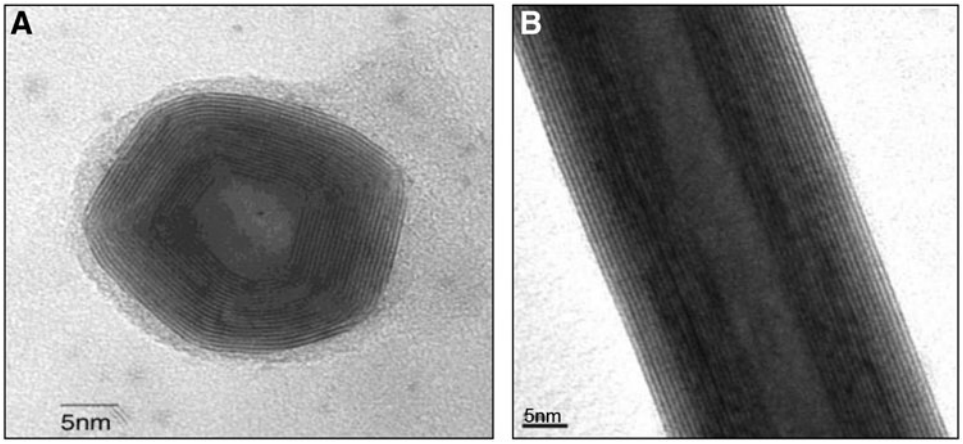

FIG. 1. Typical TEM images of **(A)** IF-WS_2 and **(B)** INT-WS_2. IF, inorganic fullerene; INT, inorganic nanotubes; TEM, transmission electron microscopy; WS_2, tungsten disulfide.

Carboxyfluorescein succinimidyl ester staining, proliferation assay, and flow cytometry

Cells were stained with carboxyfluorescein succinimidyl ester (CFSE) using CellTrace™ CFSE Cell Proliferation Kit of Molecular Probes™ according to the manufacturer's instructions with minor modifications. Briefly, cells were dissociated, suspended in Hank's balanced salt solution (HBSS) (Biological Industries) at a density of 2×10^6 cells/mL with 2.5 μM CFSE, and incubated at 37°C for 10 min. The staining was quenched with cold medium, and cells were incubated in ice (5 min), centrifuged (1100 rpm, 5 min, 17°C), and rinsed with medium twice.

Finally, the stained cells and unstained control cells were seeded in six-well tissue culture dishes at a density of 1×10^5 cells/cm^2. Twenty-four hours after the culture, the medium was changed to a fresh medium containing INT-WS_2 at different concentrations (0.22, 3.52, 35.2μg/mL). A stained control group containing no nanoparticles was seeded as well. The unstained control was tested only with the highest concentration of 35.2 μg/mL INT-WS_2 and was compared with a control group without INT-WS_2.

Twenty-four hours after the introduction of the INT-WS_2, three wells from each group were dissociated daily, for a period of 3 days, washed with phosphate-buffered saline (PBS), and analyzed by flow cytometry (accuri® C6, $\lambda=488$ nm) using FlowJo software.

Micrographs and videomicroscopy

Micrographs were taken by an Olympus inverted phase-contrast microscope (Model IX71) using a CFW 1310C camera and processed using NIH ImageJ software. The areas of the cells were measured using NIH ImageJ software.

Live videos were taken as previously described.[29] Briefly, A5 and RSC cells were seeded in 24-well tissue culture dishes at a density of 2.6×10^3 cells/cm^2, the medium of the A5/RSC experimental group was changed 24 h after culture to medium containing 35.2 μg/mL INT-WS_2 or 100 μg/mL IF-WS_2, respectively. Cells were kept at 37°C in a humidified 5% CO_2 atmosphere in a Chlamide microscope stage incubator (Live Cell Instrument). The incubator was attached to an Olympus inverted phase-contrast microscope (Model IX71). Images were obtained at 60 min intervals over a period of 72 h using a CFW 1310C camera. The automated time lapse imaging was controlled using NIH ImageJ software.

Scanning electron microscopy

For scanning electron microscopy (SEM) analysis, cells were cultured in a 24-well plate on glass microscope coverslips at a density of 2.6×10^3 cells/cm^2. The addition of the nanoparticles was done as described under ''cell growth curves and tripan blue staining.'' When the cells reached ~60% confluence, they were washed with PBS, covered with fixative containing formaldehyde and glutaraldehyde 2.5% each, in 0.1 M sodium cacodylate buffer (pH 7.4) (EMS) for 1 h, and rinsed with cacodylate (CaCo) buffer (0.1 M dimethylarsinic acid sodium salt [mercury] with 5 mM $CaCl_2$ [Merck]). The postfixation was carried out in 1% osmium tetroxide (OsO_4) (EMS) with 0.1 M CaCo buffer for 1 h; cells were dehydrated through graded ethanol concentrations (Bio-Lab). Once in 100% ethanol, the

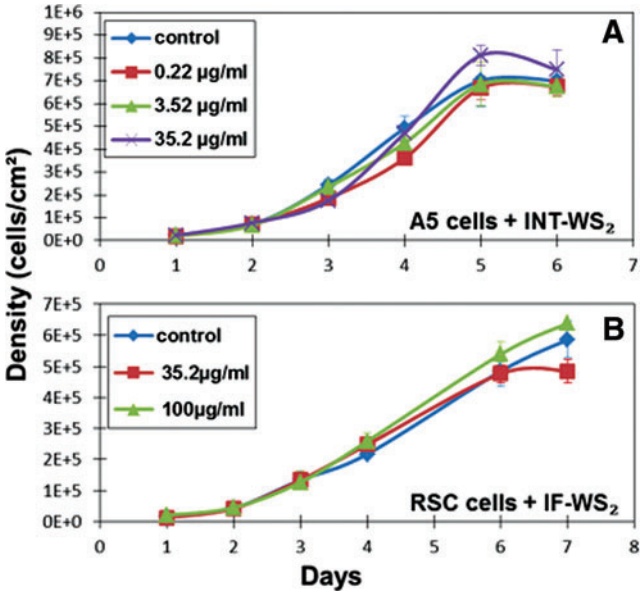

FIG. 2. Growth curves of cells with and without IF/INT-WS_2. The density variation by day of A5 **(A)** and RSC **(B)** cells cultured with different concentrations of INT-WS_2 **(A)** and IF-WS_2 **(B)** until reaching confluence. Data are expressed as the average cell density ± standard error of the mean ($n\geq4$). RSC, rat submandibular cells. Color images available online at www.liebertpub.com/tea

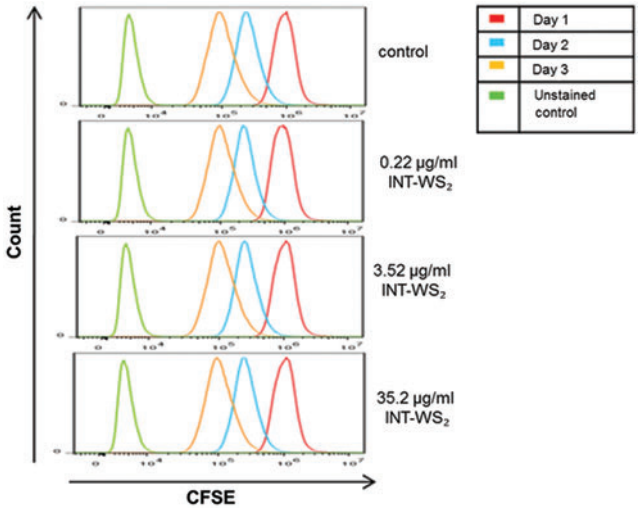

FIG. 3. CFSE proliferation assay on A5 cells with and without INT-WS_2. CFSE dilution on A5 cells cultured with different concentrations of INT-WS_2 until reaching confluence on day 3. As the cells divide, there is a reduction in the amount of fluorescence. Unstained cells have a small amount of autofluorescence as demonstrated and served as a control. Data demonstrate one representative result from three duplicates of each group with negligible standard deviations. CFSE, carboxyfluorescein succinimidyl ester. Color images available online at www.liebertpub.com/tea

mounted cells were critical-point dried in CO_2 (Bal-Tec CPD 030), mounted on aluminum sample holders with double-sided adhesive carbon tape, and sputter-coated with carbon in an Edwards 306 turbo sputter coater. The samples were analyzed with a XL30 Environmental scanning electron microscope (FEI-ESEM) using backscattered, secondary, and energy dispersive X-ray spectroscopy (EDS-EDAX instrument Phoenix) detectors.

Transmission electron microscopy

Cells were grown in 9-cm culture plates at a density of 3.1×10^2 cells/cm^2. Twenty-four hours after the culture, the medium was changed in all groups as follows: for each cell type, there was one control group and one group with nanoparticles supplemented to the medium. A5 cells were grown with 35.2 μg/mL INT-WS_2, and RSC cells were grown with 100 μg/mL IF-WS_2. Five days after the culture, the cells were fixed with fixative containing formaldehyde and glutaraldehyde 2.5% each, in 0.1 M sodium cacodylate buffer (pH 7.4) (EMS) for 2 h, and rinsed with cacodylate (CaCo) buffer (0.1 M dimethylarsinic acid sodium salt [Mercury] with 5 mM $CaCl_2$ [Merck]). Cells were then scraped, centrifuged, and embedded in 3.4% agar (Difco agar noble; Becton). Cells were postfixed in 1% OsO_4 (EMS) supplemented with potassium hexacyanoferrate trihydrate and potassium dichromate (0.5% w/v each, AnalaR;

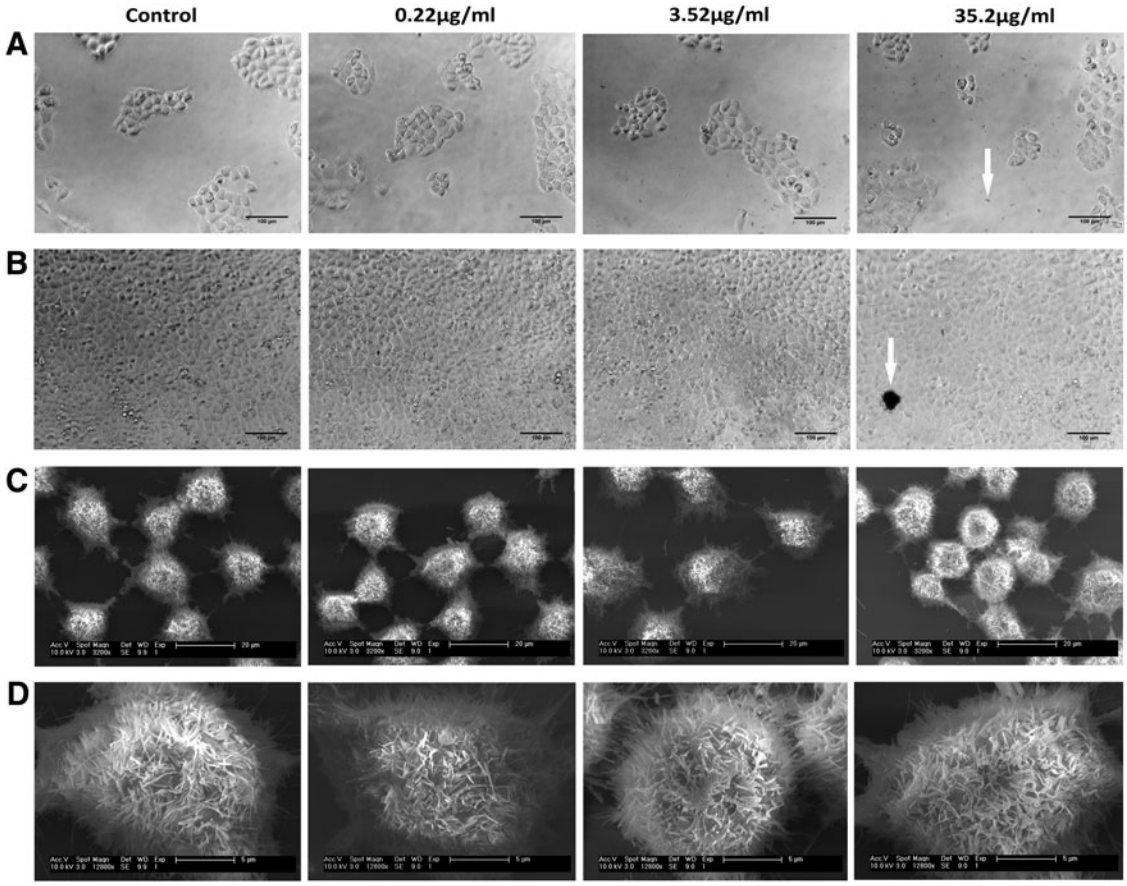

FIG. 4. A5 cells morphology is unaffected by the nanoparticles. Light microscopy **(A, B)** and SEM **(C, D)** images of A5 cells with INT-WS_2. **(A)** Second day from culture. **(B)** Fourth day from culture. *Arrow* in **(A)** indicates a single nanotube, whereas *arrow* in **(B)** most likely points to a platelet of WS_2. Scale bars: **(A, B)** 100 μm, **(C)** 20 μm, **(D)** 5 μm. SEM, scanning electron microscopy.

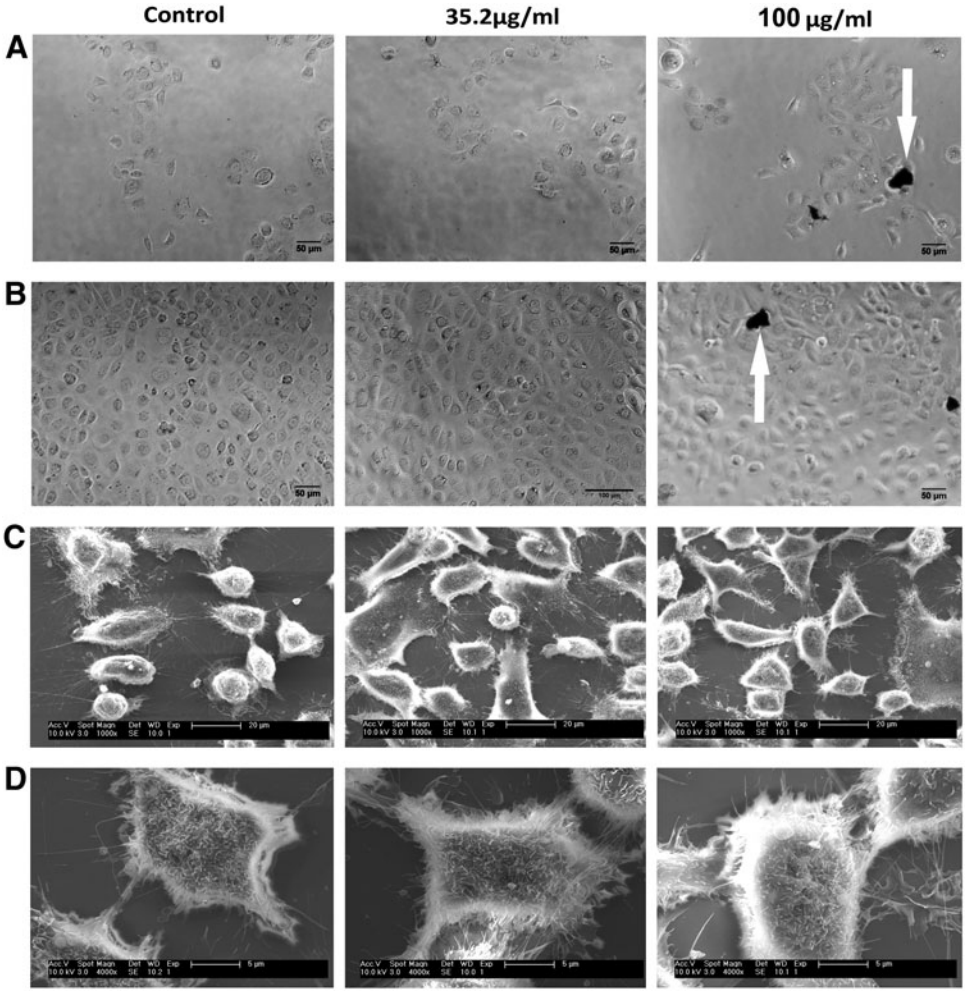

FIG. 5. RSC cells morphology is unaffected by the nanoparticles. Light microscopy **(A, B)** and SEM **(C, D)** images of RSC cells with IF-WS_2. **(A)** Second day from culture. **(B)** Fourth day from culture. The *arrows* probably point to platelets of WS_2. Scale bars: **(A, B)** 100 µm, **(C)** 20 µm, **(D)** 5 µm.

British Drug House Chemicals) in 0.1 M cacodylate (Merck) (1 h), stained with 2% uranyl acetate (EMS) in water (1 h), dehydrated in graded ethanol solutions (30–100%), and embedded in Agar 100 epoxy resin (Agar Scientific Ltd.). Ultrathin sections (70–90 nm) were prepared with ultramicrotome Leica UCT (Leica) using a diamond knife (Diatome) and analyzed with an FEI Tecnai SPIRIT (FEI; Eidhoven) transmission electron microscope operated at 120 kV and equipped with an EAGLE CCD Camera.

Statistical analysis

The Student's *t*-test was carried out for the growth curves, CFSE proliferation assays, and cell area analysis ($p < 0.05$).

Results

Cellular morphology and growth pattern

The density per day of A5 and RSC cells cultured with different concentrations of nanoparticles was measured daily with typical exponential growth curves until reaching confluence (Fig. 2). A comparison between the kinetics of the cells in the groups with different concentrations of nanoparticles indicates generally no significant differences between them (except two solitary points—on day 3, the group with 35.2 µg/mL, and on day 4, the 0.22 µg/mL group were significantly lower than the control. We believe that these results are random and therefore meaningless). Moreover, the results of the trypan blue exclusion viability test on RSC cells showed high viability (>90%) for all groups with different IF-WS_2 concentrations (data not shown).

To test whether the INT-WS_2 affect the proliferation potency of A5 cells, the CFSE proliferation assay was carried out (Fig. 3). The curves demonstrating the level of fluorescence per day are identical for all groups, indicating no significant difference in cell proliferation, and therefore, in cell viability between the different concentrations of INT-WS_2.

In all the studied groups, only a negligible overlap is found when comparing the areas under the curves on days 1 and 3, indicating that almost 100% of the cells divided during the time period measured.

To ensure that the INT-WS_2 themselves do not affect the level of fluorescence, two unstained control groups were tested: with and without INT-WS_2 (in the figure, only the unstained group without the nanoparticles is presented). The results revealed no difference between the groups (data not shown), and therefore, we conclude that the nanotubes (INT-WS_2) do not affect the fluorescence level, and the experimental results reflect differences in the cells only.

Light microscopy and SEM images of the cells with the different concentrations of nanoparticles were obtained. From the light microscopy images (Figs. 4A, B and 5A, B), it can be concluded that the cells in all groups formed normative colonies and exhibited their characteristic cobblestone appearance when reaching confluence. While analyzing the results of the SEM images, it should be noted that during the fixation procedure, the cells lose ~30% of their volume. This explains the gap observed between the cells in Figures 4C and 5C (compared with the light microscopy images). Nevertheless, the cell–cell contacts can be observed in all the groups. Two reasons for observing less nanoparticles in the SEM images compared with the light microscopy (for the same concentrations) are as follows: (1) during the SEM fixation procedure, most of the nanoparticles in the medium are washed out and (2) the nanoparticles deep inside the cells cannot be observed by the secondary detector. In Figures 4D and 5D, a representative single cell from each group is demonstrated at higher magnification enabling observation of the membrane protrusions of the cells: microvilli, surface ruffling, and lamellipodium. In addition, secretory granules, typical for these type of secretory epithelium cells, can be observed. No significant difference in morphology between the groups tested was observed (Figs. 4 and 5).

We further analyzed the area of the cells from the different groups. The results are presented in Figure 6 and indicate no significant difference in the area of the cells. The cells with and without the nanoparticles were observed continuously during culture by videomicroscopy. The Supplementary Videos S1–S4 (Supplementary Data are available online at www.liebertpub.com/tea) indicate that even the cells with the highest concentration (of 35.2 μg/mL INT-WS_2 for A5 cells, and 100 μg/mL IF-WS_2 for RSC cells) proliferated and spread out normally and were insensitive to the nanoparticles in the medium.

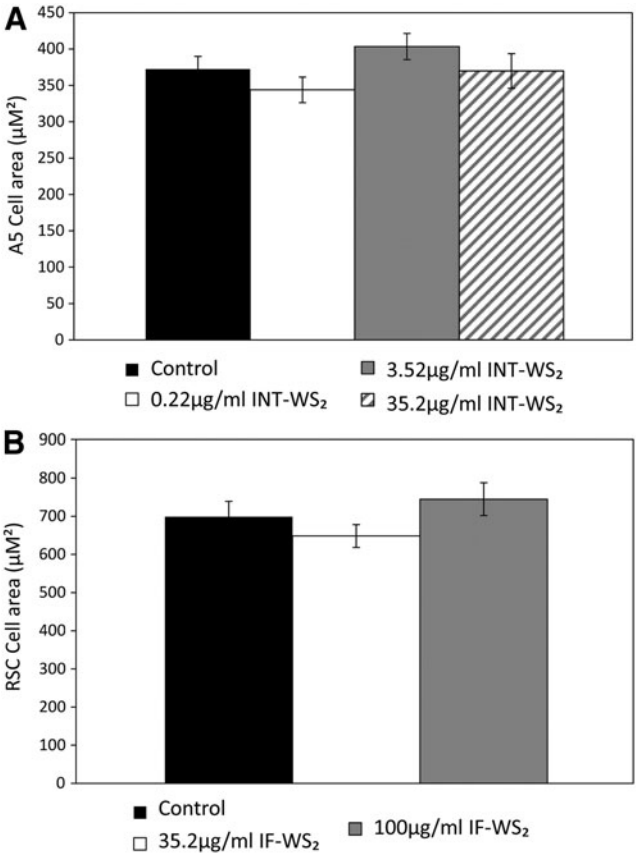

FIG. 6. The cellular area of A5 and RSC cells with/without the nanoparticles. Light microscopy images of A5 cells **(A)** and RSC cells **(B)** upon reaching confluence (day 5 for A5 cells and day 4 for RSC cells) were analyzed. Cells were chosen in a random manner from each image and measured using NIH ImageJ software. Data are expressed as the average cell area ± standard error of the mean (number of cells = 35).

The interaction of IF/INT-WS_2 with the cells

We further investigated the specific interaction between the nanoparticles and the cells on a single-cell level. To do so, we took advantage of different detectors available in the SEM: secondary (SE), backscatter (BSE), and the EDS and analyzed the samples from the group with the highest nanoparticle concentration of 35.2 μg/mL for A5 cells and 100 μg/mL for RSC cells.

To locate the areas containing the nanoparticles on the sample, we used the BSE detector at relatively low magnification. The advantage of the BSE detector is the maximization of the contrast between the nanoparticles (which present a brighter signal) and the rest of the biological sample.

Next, the cells, which BSE analysis found to be in contact with the nanoparticles, were examined under higher magnification and resolution using SE detector. To ensure that the higher signal detected is indeed the IF/INT-WS_2, we used EDS, as presented in Figures 7 and 8.

Figures 7 and 8 present cells grown in a medium containing 35.2 μg/mL INT-WS_2 or 100 μg/mL IF-WS_2, respectively. Two locations are marked on the cells: Area (1) is a control without nanoparticles, in correlation with the EDS presented in Figures 7 and 8(B1), which shows negligible peaks for the tungsten (W) and sulfur (S) components. Area (2) is probably located on the nanoparticles, as verified on the EDS in Figures 7 and 8(B2), where peaks of W and S components are observed. These results clearly indicate that the areas with higher signal presented by the BSE detector are indeed the nanoparticles.

Figures 7 and 8 also show that there is a contact between the cells and the nanoparticles, although the resolution does not enable the determination of whether the nanoparticles penetrate the cells or only bind to the external part of the cell membrane. To investigate the capability of the nanoparticles to enter the cells, transmission electron microscopy (TEM) was utilized (Figs. 9 and 10). Interestingly, the nanoparticles were seen inside the cells, implying the uptake of the IF/INT-WS_2 by the cells. Moreover, nanoparticles were not observed in the cellular nucleus, but rather in their cytoplasm—in most cases surrounded by a membrane. In some of the images, WS_2 platelets, a byproduct of the synthesis, were observed inside the lysosome organelles [Fig. 9(III)]. Interestingly, despite the internalization of the nanoparticles, the organelles remained intact [Figs. 9 and 10(II–VI)].

Discussion

This study involves INT-WS_2 and IF-WS_2. These nanoparticles were found to be beneficial for many diverse

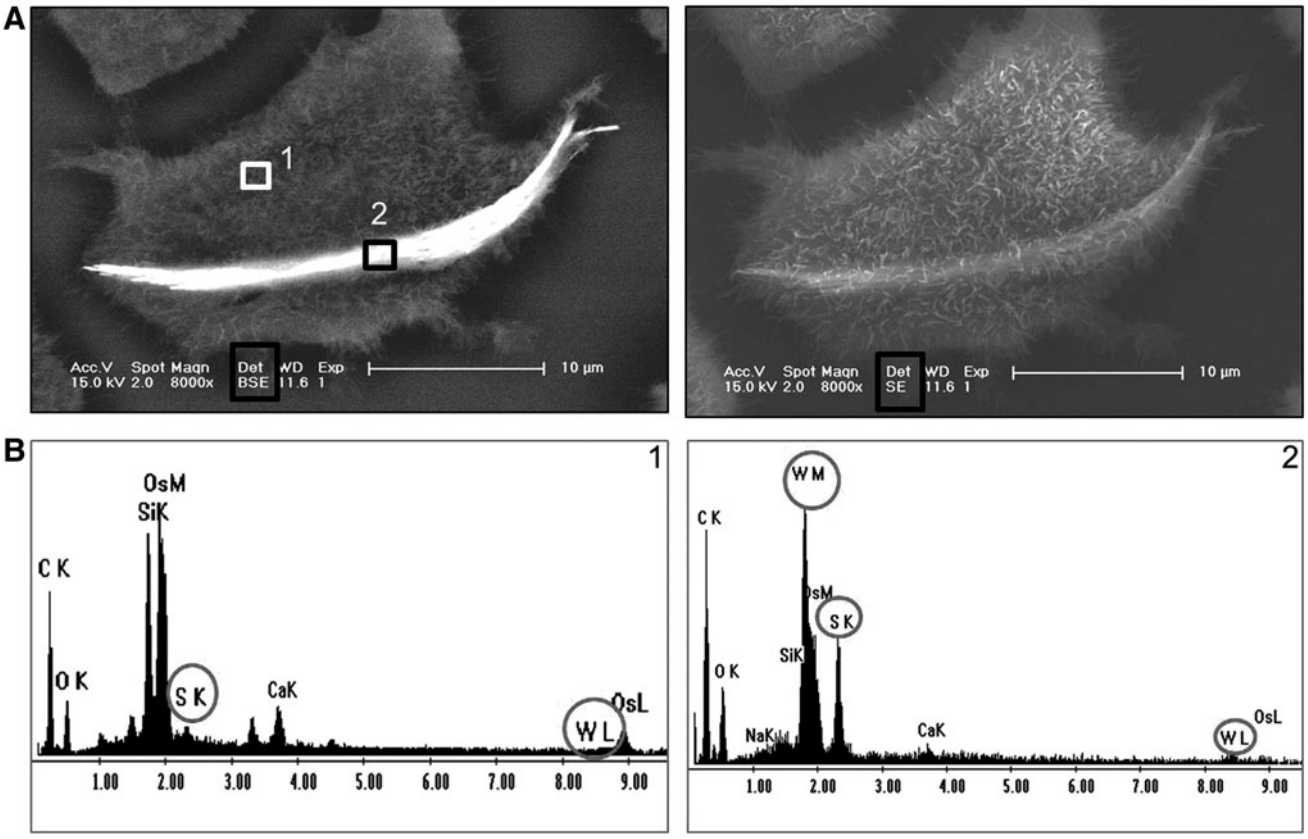

FIG. 7. Contact between A5 cells and INT-WS_2. **(A)** Environmental scanning electron microscopy (ESEM) images (using backscattered (BSE) and secondary (SE) detectors as indicated in the *black box*) of an A5 cell grown in a medium with 35.2 µg/mL INT-WS_2. The EDS of areas **1** (*white rectangle*, control) and **2** (*black rectangle*, nanotube aggregate) are shown in *panel* **(B)**. The compounds, tungsten (W, M, and L shells) and sulfur (S and K shells), show peaks in the EDS of **(B2)**—area of cell in contact with nanotube but do not appear in **(B1)**—control area of cell. EDS, energy dispersive X-ray spectroscopy.

medical applications,[11] among them, re-enforcement of scaffolds for tissue engineering[39] highlighting the need for verification of their biocompatibility. Consequently, our aim was to examine whether IF/INT-WS_2 are biocompatible on A5 and RSC SG cells. This platform may contribute to possible future applications of these nanoparticles on SG-related disorders, such as drug delivery systems, re-enforcement of scaffolds for tissue engineering, biomedical coatings and gels, cancer hypothermia treatment, and imaging contrast agents. The question whether these ideas are practical or not depends first and foremost on the biocompatibility of nanoparticles and hence the significance of this study.

We tested the effect of IF/INT-WS_2 on three different aspects of the cells: their viability (proliferation), morphology, and the direct interaction between the nanotubes and the cells. We randomly chose to test the effect of IF-WS_2 on RSC cells and INT-WS_2 (nanotubes) on A5 cells. For A5 cells, three concentrations of INT-WS_2 were chosen for the experiments besides the control. Concentrations of 0.22 and 3.52 µg/mL were chosen according to a previous study with IF-MoS_2.[21] To ensure no cytotoxic effects on the cells, we added an additional concentration, multiplied by 10-fold, of 35.2 µg/mL. For the RSC cells, we chose two concentrations of IF-WS_2: 35.2 µg/mL as the highest concentration, which was used for A5 cells, and another high concentration of 100 µg/mL, which is the highest concentration studied for the assessment of the biocompatibility of BNNT.[40] The IF/INT-WS_2 tend to agglomerate, and therefore, the cells were exposed to a mixture of single nanoparticles together with aggregates.

Growth curves (Fig. 2) demonstrate the whole culture growth cycle: lag, exponential, and plateau phases and enable the detection of any deviations in a specific part of the curve. The combination of the trypan blue assay improves the accuracy of the growth curves by excluding the stained dead cells. The proliferation assay (Fig. 3), on the other hand, does not describe the whole cycle since the limitations of the flow cytometer require a higher concentration of cells to begin with. However, it is more accurate than manual counting and reveals information of the fluorescence per cell enabling the detection of the percentage of cells that underwent divisions.

The results clearly indicated that the IF/INT-WS_2 induced no significant difference on the kinetics, viability, and proliferation capability of the cells at all concentrations tested.

Light microscopy (Figs. 4 and 5) demonstrates the general shape of the cells and the clones that the cells form, which can be seen ''live'' on the videomicroscopy (Supplementary Videos S1–S4), whereas SEM images (Figs. 4 and 5) exhibit mainly the cell membrane morphology at a higher resolution. The area of the cells was analyzed as well

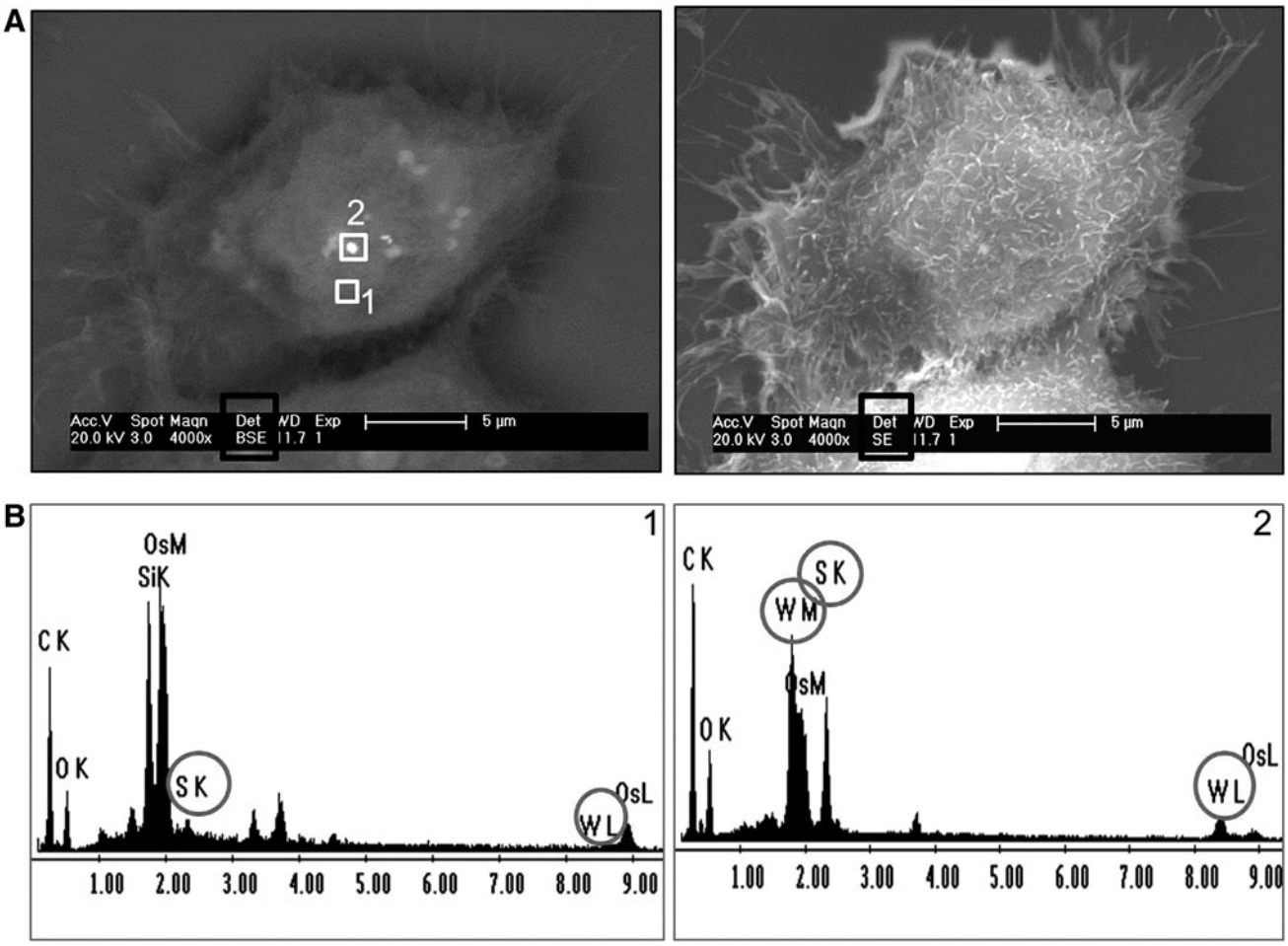

FIG. 8. Contact between a RSC cell and IF-WS_2. **(A)** ESEM images (using BSE and SE detectors as indicated in the *black box*) of a RSC cell grown in a medium with 100 µg/mL IF-WS_2. The EDS of areas **1** (control) and **2** (IF-WS_2) are shown in panel **(B)**. The elements tungsten (W, M, and L shells) and sulfur (S and K shells) show peaks in the EDS of **(B2)**—area of cell in contact with the nanoparticle but do not appear in **(B1)**—control area of cell.

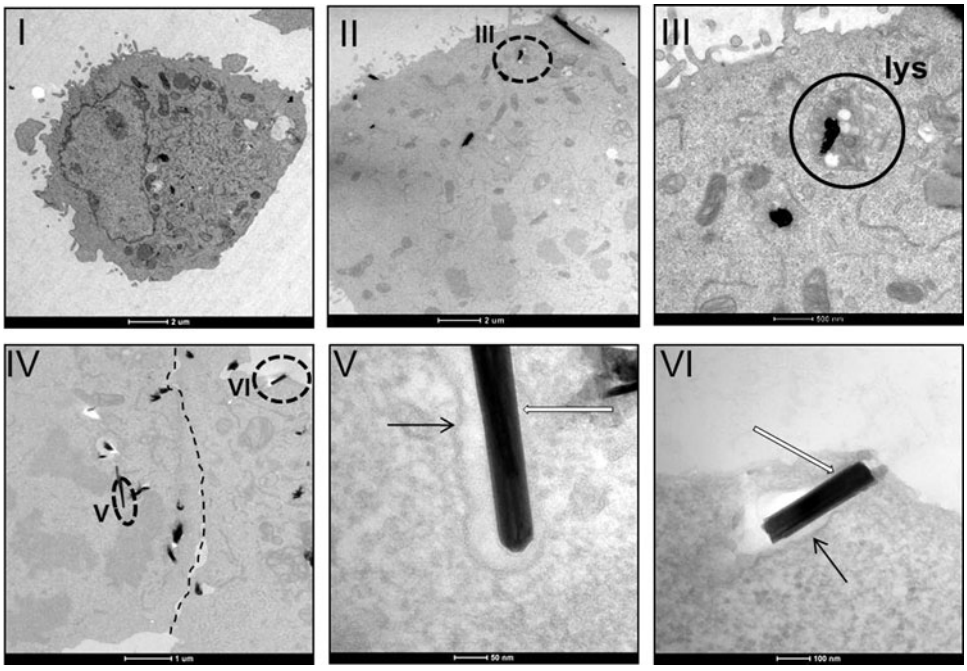

FIG. 9. INT-WS_2 are uptaken by A5 cells. TEM images of A5 cells without **(I)** or with **(II–VI)** 35.2 µg/mL INT-WS_2. The *dashed circles* delimit an area that is enlarged in another panel (as indicated). The *white arrows* are pointing at the nanoparticles, whereas the *black arrows* show the intracellular membrane surrounding them. The *dashed line* in panel **(IV)** is located on a tight junction between two cells.

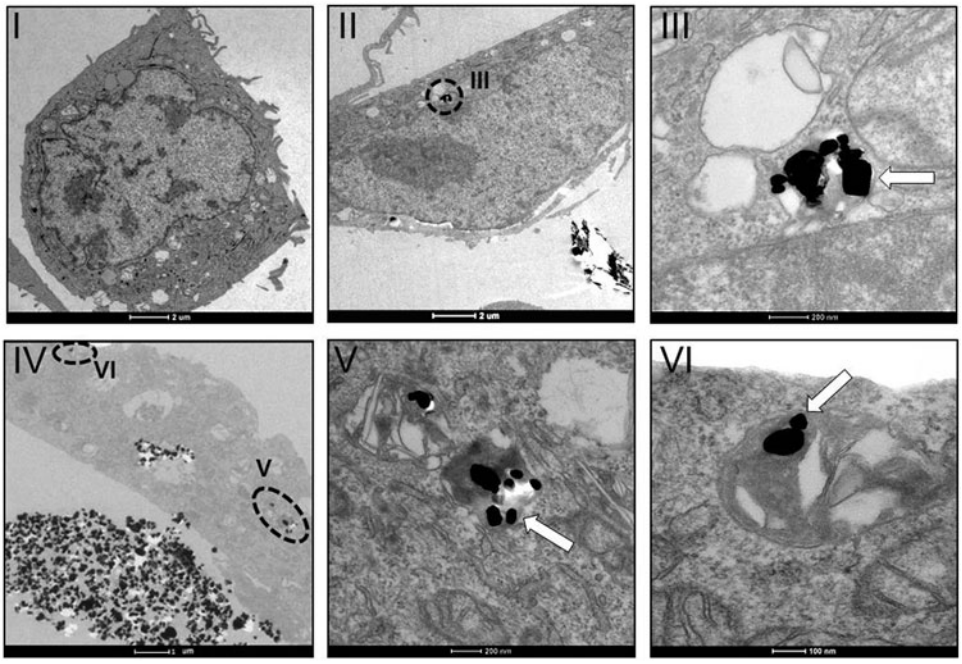

FIG. 10. IF-WS_2 are uptaken by RSC cells. TEM images of RSC cells without **(I)** or with **(II–VI)** 100 μg/mL IF-WS_2. The *dashed circles* delimit an area that is enlarged in another panel (as indicated). The *white arrows* pointing to nanoparticle aggregates.

(Fig. 6). These results further indicate that the IF/INT-WS_2, in all concentrations tested, did not affect neither the cellular morphology and size nor the cells clone formation pattern. These positive results are preliminary and lead to the need of further investigation, such as toxicology tests exploring reactive oxygen species formation as well as nanoparticle–proteins interaction. Moreover, some future studies should be designed to assess the cellular response to nanoparticle embedded in a surface (rather than in suspension) and *in vivo* studies relating the issues of immune response and fibrosis to address applications, such as scaffold reenforcement.

An interesting finding was the ability of the cells to uptake the nanoparticles. A contact between the cells and the nanoparticles was clearly observed by EDS analysis (Figs. 7 and 8), although the resolution does not enable the determination of whether the nanoparticles penetrate the cells or only bind to the external component of the cell membrane.

TEM analysis [Figs. 9 and 10(II–VI)] further demonstrated the ability of A5 and RSC cells to uptake INT-WS_2 and IF-WS_2, respectively. The nanoparticles were located in the cytoplasm of cells, but not in the nuclei, and were surrounded in most cases by a membrane, which may indicate a mechanism of endocytosis. This assumption is reinforced by some of the images where the nanoparticles seem to be engulfed by the cells [Fig. 9(IV,VI)]. It is important to note that despite the presence of nanoparticles inside the cells, comparison of micrographs of control and treated cell organelles indicated that the cells are intact. Whereas these preliminary experiments are good indication of the biocompatibility of these nanoparticles, further work with better statistical analysis is needed to form sound conclusions about their intracellular localization. Moreover, the extent, kinetics, and exact mechanism, as well as the ability of nanoparticles to exit the cells are yet to be determined. Interestingly, several different studies revealed that cells can engulf BNNTs,[9,19,40,41] INT-WS_2, and IF-MoS_2.[24] Indeed, these nanoparticles were found incorporated inside cytoplasmic vesicles, but not inside the nuclei. The internalization of the BNNTs was shown to be energy dependent, indicating the mechanism of endocytosis. In these studies and in agreement with our study, the nanoparticles were not structurally altered and were found to be nontoxic for the cells despite their ability to penetrate them. In other studies, cellular uptake of BNNT (Horvath *et al.*, 2011)[42] was found to be toxic. In other studies, complexes of siRNA conjugated to nanoparticles (composed of diblock polymers) in the size of 50–60 nm ($\sim$1/2 the size of IF/INT-WS_2) were uptaken by SG cells *in vitro* and *in vivo* by the mechanism of endocytosis.[43,44] Nanoparticle uptake by cells was indeed previously studied for several types of nanoparticles and cell types, and the results reveal that cellular nanoparticle uptake *in vitro* is a common phenomenon.[45–50] The extent, mechanism of cell entry, and subcellular localization of nanoparticles internalized by cells are dependent on several factors, such as the nanoparticle size, surface modifications, structure, morphology, charge, and level of hydrophilicity. In addition, the same nanoparticles can behave differently depending on the type of cells studied. Yet it should be noted that as in most *in vitro* studies, these results should be regarded with circumspection. There may be fundamental differences in nanoparticle uptake when comparing *in vitro* and *in vivo* assays. For instance, nanoparticles were efficiently engulfed by the mononuclear phagocyte system,[44] but this cannot be directly compared to cultured cells, which contain one type of cell exposed to high nanoparticle concentration in the medium.

Conclusions

This study provides experimental evidence for the biocompatibility of IF/INT-WS_2, as measured by the exposed viability and morphology of the cells. We have further established the propensity of the nanoparticles to penetrate to

the cell interior. Nanoparticle uptake can be either advantageous or a drawback, depending on the desired application.[45] Therefore, these results are encouraging for future medical applications of these nanoparticles, especially as specific drug delivery carriers or imaging contrast agents. The biocompatibility of IF/INT-WS_2 with SG, as shown in this study, portends many promising future medical applications for various SG disorders, such as re-enforcement of scaffolds for tissue engineering, drug delivery agents, biomedical coatings and gels, cancer hypothermia treatment, and imaging contrast agents. Nevertheless, more *in vitro* and *in vivo* biocompatibility studies should be utilized.

Acknowledgments

The electron microscopy studies were conducted at the Irving and Cherna Moskowitz Center for Nano and Bio-Nano Imaging at the Weizmann Institute of Science. We are grateful to Dr. I. Sabanay and Dr. V. Shinder for TEM consulting and to Dr. S.R. Cohen for critical review of the article. R.T. acknowledges the support of the ERC support through MEDIF-2 PoC project and the KAMIN project of the Office of Chief Scientist, Israeli Ministry of Economy.

Disclosure Statement

No competing financial interests exist.

References

1. Fakruddin, M., Hossain, Z., and Afroz, H. Prospects and applications of nanobiotechnology: a medical perspective. J Nanobiotechnol **10,** 31, 2012.
2. Margulis, L., Salitra, G., Tenne, R., and Talianker, M. Nested fullerene-like structures. Nature **365,** 113, 1993.
3. Tenne, R., Margulis, L., Genut, M., and Hodes, G. Polyhedral and cylindrical structures of tungsten disulfide. Nature **360,** 444, 1992.
4. Tenne, R. Inorganic nanotubes and fullerene-like nanoparticles. Nat Nanotechnol **1,** 103, 2006.
5. Rapoport, L., Bilik, Y., Feldman, Y., Homyonfer, M., Cohen, S.R., and Tenne, R. Hollow nanoparticles of WS2 as potential solid-state lubricants. Nature **387,** 791, 1997.
6. Cizaire, L., Vacher, B., Le Mogne, T., Martin, J.M., Rapoport, L., Margolin, A., *et al.* Mechanisms of ultra-low friction by hollow inorganic fullerene-like MoS2 nanoparticles. Surf Coat Tech **160,** 282, 2002.
7. Rosentsveig, R., Gorodnev, A., Feuerstein, N., Friedman, H., Zak, A., Fleischer, N., *et al.* Fullerene-like MoS2 nanoparticles and their tribological behavior. Tribol Lett **36,** 175, 2009.
8. Zhi, C., Bando, Y., Tang, C., and Golberg, D. Immobilization of proteins on boron nitride nanotubes. J Am Chem Soc **127,** 17144, 2005.
9. Chen, X., Wu, P., Rousseas, M., Okawa, D., Gartner, Z., Zettl, A., *et al.* Boron nitride nanotubes are noncytotoxic and can be functionalized for interaction with proteins and cells. J Am Chem Soc **131,** 890, 2009.
10. Tahir, M.N., Yella, A., Sahoo, J.K., Annal-Therese, H., Zink, N., and Tremel, W. Synthesis and functionalization of chalcogenide nanotubes. Phys Status Solidi B **247,** 2338, 2010.
11. Adini, A.R., Redlich, M., and Tenne, R. Medical applications of inorganic fullerene-like nanoparticles. J Mater Chem **21,** 15121, 2011.
12. Lee, C., Hong, C., Kim, H., Kang, J., and Zheng, H.M. TiO2 nanotubes as a therapeutic agent for cancer thermotherapy. Photochem Photobiol **86,** 981, 2010.
13. Lalwani, G., Henslee, A.M., Farshid, B., Parmar, P., Lin, L., Qin, Y.X., *et al.* Tungsten disulfide nanotubes reinforced biodegradable polymers for bone tissue engineering. Acta Biomater **9,** 8365, 2013.
14. Tan, A.W., Pingguan-Murphy, B., Ahmad, R., and Akbar, S.A. Review of titania nanotubes: fabrication and cellular response. Ceram Int **38,** 4421, 2012.
15. Goldbart, O., Sedova, A., Yadgarov, L., Rosentsveig, R., Shumalinsky, D., Lobik, L., *et al.* Lubricating medical devices with fullerene-like nanoparticles. Tribol Lett **55,** 103, 2014.
16. Samorodnitzky-Naveh, G.R., Redlich, M., Rapoport, L., Feldman, Y., and Tenne, R. Inorganic fullerene-like tungsten disulfide nanocoating for friction reduction of nickel-titanium alloys. Nanomedicine **4,** 943, 2009.
17. Ron, R., Zbaida, D., Kafka, I.Z., Rosentsveig, R., Leibovitch, I., and Tenne, R. Attenuation of encrustation by self-assembled inorganic fullerene-like nanoparticles. Nanoscale **6,** 5251, 2014.
18. Chen, R., So, M.H., Yang, J., Deng, F., Che, C.M., and Sun, H. Fabrication of bismuth subcarbonate nanotube arrays from bismuth citrate. Chem Commun (Camb) 2265, 2006.
19. Ciofani, G., Danti, S., D'Alessandro, D., Ricotti, L., Moscato, S., Bertoni, G., *et al.* Enhancement of neurite outgrowth in neuronal-like cells following boron nitride nanotube-mediated stimulation. ACS Nano **4,** 6267, 2010.
20. Ciofani, G., Danti, S., Genchi, G.G., Mazzolai, B., and Mattoli, V. Boron nitride nanotubes: biocompatibility and potential spill-over in nanomedicine. Small **9,** 1672, 2013.
21. Wu, H.H., Yang, R., Song, B.M., Han, Q.S., Li, J.Y., Zhang, Y., *et al.* Biocompatible inorganic fullerene-like molybdenum disulfide nanoparticles produced by pulsed laser ablation in water. ACS Nano **5,** 1276, 2011.
22. Corazzari, I., Deorsola, F.A., Gulino, G., Aldieri, E., Bensaid, S., Turci, F., *et al.* Hazard assessment of W and Mo sulphide nanomaterials for automotive use. J Nanopart Res **16,** 2401, 2014.
23. Teo, W.Z., Chng, E.L., Sofer, Z., and Pumera, M. Cytotoxicity of exfoliated transition-metal dichalcogenides (MoS2, WS2, and WSe2) is lower than that of graphene and its analogues. Chemistry **20,** 9627, 2014.
24. Pardo, M., Shuster-Meiseles, T., Levin-Zaidman, S., Rudich, A., and Rudich, Y. Low cytotoxicity of inorganic nanotubes and fullerene-like nanostructures in human bronchial epithelial cells: relation to inflammatory gene induction and antioxidant response. Environ Sci Technol **48,** 3457, 2014.
25. Pardo, M., Shuster-Meiseles, T., Levin-Zaidman, S., Rudich, A., and Rudich, Y. Low cytotoxicity of inorganic nanotubes and fullerene-like nanostructures in human bronchial epithelial cells: relation to inflammatory gene induction and antioxidant response. Environ Sci Technol **48,** 3457, 2014.
26. Aframian, D.J., and Palmon, A. Current status of the development of an artificial salivary gland. Tissue Eng Part B Rev **14,** 187, 2008.
27. Aframian, D.J., Tran, S.D., Cukierman, E., Yamada, K.M., and Baum, B.J. Absence of tight junction formation in an allogeneic graft cell line used for developing an engineered artificial salivary gland. Tissue Eng **8,** 871, 2002.

28. David, R., Shai, E., Aframian, D.J., and Palmon, A. Isolation and cultivation of integrin alpha(6)beta(1)-expressing salivary gland graft cells: a model for use with an artificial salivary gland. Tissue Eng Part A **14,** 331, 2008.
29. Yaniv, A., Neumann, Y., David, R., Stiubea-Cohen, R., Orbach, Y., Lang, S., *et al.* Establishment of immortal multipotent rat salivary progenitor cell line toward salivary gland regeneration. Tissue Eng Part C Methods **17,** 69, 2011.
30. Aframian, D.J., David, R., Ben-Bassat, H., Shai, E., Deutsch, D., Baum, B.J., *et al.* Characterization of murine autologous salivary gland graft cells: a model for use with an artificial salivary gland. Tissue Eng **10,** 914, 2004.
31. Neumann, Y., David, R., Stiubea-Cohen, R., Orbach, Y., Aframian, D.J., and Palmon, A. Long-term cryopreservation model of rat salivary gland stem cells for future therapy in irradiated head and neck cancer patients. Tissue Eng Part C Methods **18,** 710, 2012.
32. Aframian, D.J., Cukierman, E., Nikolovski, J., Mooney, D.J., Yamada, K.M., and Baum, B.J. The growth and morphological behavior of salivary epithelial cells on matrix protein-coated biodegradable substrata. Tissue Eng **6,** 209, 2000.
33. Aframian, D.J., Redman, R.S., Yamano, S., Nikolovski, J., Cukierman, E., Yamada, K.M., *et al.* Tissue compatibility of two biodegradable tubular scaffolds implanted adjacent to skin or buccal mucosa in mice. Tissue Eng **8,** 649, 2002.
34. Aframian, D.J., Zheng, C., Goldsmith, C.M., Nikolovski, J., Cukierman, E., Yamada, K.M., *et al.* Using HSV-thymidine kinase for safety in an allogeneic salivary graft cell line. Tissue Eng **7,** 405, 2001.
35. Brown, A.M., Rusnock, E.J., Sciubba, J.J., and Baum, B.J. Establishment and characterization of an epithelial cell line from the rat submandibular gland. J Oral Pathol Med **18,** 206, 1989.
36. Zak, A., Sallacan-Ecker, L., Margolin, A., Genut, M., and Tenne, R. Insight into the growth mechanism of Ws2 nanotubes in the scaled-up fluidized-bed reactor. Nano **4,** 91, 2009.
37. Feldman, Y., Frey, G.L., Homyonfer, M., Lyakhovitskaya, V., Margulis, L., Cohen, H., *et al.* Bulk synthesis of inorganic fullerene-like MS(2) (M = Mo, W) from the respective trioxides and the reaction mechanism. J Am Chem Soc **118,** 5362, 1996.
38. Aframian, D.J., Amit, D., David, R., Shai, E., Deutsch, D., Honigman, A., *et al.* Reengineering salivary gland cells to enhance protein secretion for use in developing artificial salivary gland device. Tissue Eng **13,** 995, 2007.
39. Lalwani, G., Henslee, A.M., Farshid, B., Lin, L., Kasper, F.K., Qin, Y.X., *et al.* Two-dimensional nanostructure-reinforced biodegradable polymeric nanocomposites for bone tissue engineering. Biomacromolecules **14,** 900, 2013.
40. Ciofani, G., Ricotti, L., Danti, S., Moscato, S., Nesti, C., D'Alessandro, D., *et al.* Investigation of interactions between poly-L-lysine-coated boron nitride nanotubes and C2C12 cells: up-take, cytocompatibility, and differentiation. Int J Nanomed **5,** 285, 2010.
41. Ciofani, G., Raffa, V., Menciassi, A., and Cuschieri, A. Cytocompatibility, interactions, and uptake of polyethyleneimine-coated boron nitride nanotubes by living cells: confirmation of their potential for biomedical applications. Biotechnol Bioeng **101,** 850, 2008.
42. Horvath, L., Magrez, A., Golberg, D., *et al.* In vitro investigation of the cellular toxicity of boron nitride nanotubes. ACS nano **5,** 3800, 2011.
43. Arany, S., Xu, Q., Hernady, E., Benoit, D.S., Dewhurst, S., and Ovitt, C.E. Pro-apoptotic gene knockdown mediated by nanocomplexed siRNA reduces radiation damage in primary salivary gland cultures. J Cell Biochem **113,** 1955, 2012.
44. Arany, S., Benoit, D.S., Dewhurst, S., and Ovitt, C.E. Nanoparticle-mediated gene silencing confers radioprotection to salivary glands *in vivo*. Mol Ther **21,** 1182, 2013.
45. Park, M.V., Lankveld, D.P., van Loveren, H., and de Jong, W.H. The status of *in vitro* toxicity studies in the risk assessment of nanomaterials. Nanomedicine (Lond) **4,** 669, 2009.
46. Mailander, V., and Landfester, K. Interaction of nanoparticles with cells. Biomacromolecules **10,** 2379, 2009.
47. Geisberger, G., Paulus, S., Gyenge, E.B., Maake, C., and Patzke, G.R. Targeted delivery of polyoxometalate nanocomposites. Small **7,** 2808, 2011.
48. Zhai, X., Yu, M., Cheng, Z., Hou, Z., Ma, P., Yang, D., *et al.* Rattle-type hollow CaWO4:Tb(3+)@SiO2 nanocapsules as carriers for drug delivery. Dalton Trans **40,** 12818, 2011.
49. Kuhnel, D., Busch, W., Meissner, T., Springer, A., Potthoff, A., Richter, V., *et al.* Agglomeration of tungsten carbide nanoparticles in exposure medium does not prevent uptake and toxicity toward a rainbow trout gill cell line. Aquat Toxicol **93,** 91, 2009.
50. Coulter, J.A., Jain, S., Butterworth, K.T., Taggart, L.E., Dickson, G.R., McMahon, S.J., *et al.* Cell type-dependent uptake, localization, and cytotoxicity of 1.9 nm gold nanoparticles. Int J Nanomed **7,** 2673, 2012.

Address correspondence to:
Doron J. Aframian, DMD, PhD
Salivary Gland Clinic and Diagnostic Laboratory
Department of Oral Medicine
The Hebrew University-Hadassah School
of Dental Medicine
P.O.B 12272
Jerusalem 91120
Israel

E-mail: dorona@hadassah.org.il

Received: March 16, 2014
Accepted: October 7, 2014
Online Publication Date: December 18, 2014